Stability Analysis of Traffic Control in Two-region Urban Cities

Jack Haddad

Nikolas Geroliminis

STRC 2011 **May 2011**

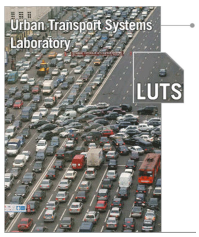

ÉCOLE POLYTECHNIQUE
FÉDÉRALE DE LAUSANNE

STRC 2011

Stability Analysis of Traffic Control in Two-region Urban Cities

Jack Haddad
ÉCOLE POLYTECHNIQUE FÉDÉRALE DE LAUSANNE (EPFL)
School of Architecture, Civil and Environmental Engineering (ENAC)
Urban Transport Systems Laboratory (LUTS)
phone: +41 21 6935397
fax: +41 21 6935397
jack.haddad@epfl.ch

Nikolas Geroliminis
ÉCOLE POLYTECHNIQUE FÉDÉRALE DE LAUSANNE (EPFL)
School of Architecture, Civil and Environmental Engineering (ENAC)
Urban Transport Systems Laboratory (LUTS)
phone: +41 21 6932481
fax: +41 21 6932481
nikolas.geroliminis@epfl.ch

May 2011

Abstract

In this paper, stability analysis of traffic control for two-region urban cities is treated. Two Macroscopic Fundamental Diagrams (MFDs) system for two regions is defined. Under the assumption of triangle MFDs, and two traffic demands: exogenous and endogenous demands, the two-region MFDs system is modeled as a piecewise second-order system. Necessary and sufficient conditions are derived for stable equilibrium accumulations in the undersaturated regimes for both MFDs. Moreover, the traffic perimeter control problem for the two-region MFDs system is formulated. Phase portraits and stability analysis are conducted, and new algorithm is proposed to derive the boundaries of the stable and unstable regions. Based on these regions, a state-feedback control strategy is derived. Few numerical examples are presented.

Keywords

stability characterization, macroscopic fundamental diagram, state-feedback control

1 Introduction

As traffic congestion increases in urban cities, an aggregate model approach that considers the traffic dynamics of a large urban area is promising in alleviating congestion. A macroscopic fundamental diagram (MFD) links space-mean flow, density, and speed of a large urban area. Under the assumption that average trip length from all origins is constant with time, the MFD links *accumulation* [veh] $n(t)$ [veh], defined as the number of vehicles in the network at time t, and *exit flow* [veh/sec] $G(n)$ [veh/sec], defined as the rate vehicles reach their destinations, Daganzo (2007).

Management and control of multi-region macroscopic fundamental diagrams (MFDs) system can improve urban mobility, prevent overcrowding, and relieve congestion in cities.

The existing of a well-defined MFD for urban network was shown by microscopic simulation of the San Francisco Business District, Geroliminis (2007), and experimentally revealed in Yokohama (Japan), Geroliminis and Daganzo (2008). Analytical theories for urban MFD were derived in Daganzo and Geroliminis (2008) and Helbing (2009), using a density-based and a utilization-based approach, respectively.

Recent findings from empirical, Geroliminis and Sun (2011), and simulated data, Mazloumian *et al.* (2010), show that the spatial variability of vehicle density is a key variable that affects the shape, the scatter, and the existence of a well-defined MFD, e.g. when the link density variance over all links in the network is low the scatter of an MFD is low. Moreover, the effect of link lengths, incoming turns, and signal timing, i.e. cycle length, proportion of green light, and offsets, are shown in Boyacı and Geroliminis (2011) based on the variational theory, Daganzo (2005).

The concept of having a traffic network with a well-defined MFD can be utilized to control the exit flow by managing and controlling the network accumulation. Moreover, if the network has heterogeneous demand then one can partition the network to homogeneous regions with small variances of link densities as each region will have a well-defined MFD. In Ji and Geroliminis (2011), a clustering algorithm for heterogeneous transportation networks to homogeneous regions is presented.

The optimal control policy was derived for a single MFD system, while the optimality principles of control were only introduced for multi-region MFDs system in Daganzo (2007). The control strategies aim to decrease inflows in regions with points in the decreased part of an MFD, and manage the accumulation to maintain the flow in the city on its maximum.

Stability analysis and control synthesis of a nonlinear system are not a trivial task. Even for a simple class of nonlinear system such as piecewise affine systems, and despite the fact that

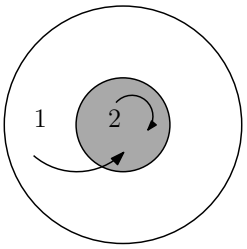

Figure 1: System of two MFDs with two state variables, e.g. periphery of the center (1) and city center (2).

piecewise affine models are just a composition of linear dynamic systems, their stability properties are complex and cannot be easily deduced from those of the component linear subsystems, and instead, numerical tests were proposed in Bemporad *et al.* (2000).

In this paper, the stability analysis for two-region MFDs system is treated, where the dynamics equations are formulated as a piecewise second-order system. The MFDs are assumed to be in triangle shapes, and the two regions have two traffic demands: one region has an exogenous demand, i.e. all the trips generated have external destinations, e.g. the periphery of the city center generates trips to the city center, while the other region has an endogenous demand, i.e. all the trips have internal destinations, e.g. the city center attracts all trips. Furthermore, necessary and sufficient conditions are derived for stable equilibrium point in the undersaturated regimes for both MFDs. A new algorithm is proposed for computing the boundaries of stable and unstable regions. Finally, a state-feedback control is derived where the criterion is to maximize the output of the system, i.e. the number of vehicles that complete their trips and reach their destinations.

This paper is organized as follows: the dynamic equations and the control problem for two-region MFDs system are formulated in Section 2, and also phase portraits for piecewise second-order system is conducted. In Section 3 stability analysis and new algorithm for computing the boundaries of the stable and unstable regions is proposed. The state-feedback control law is presented in Section 4.

2 Two-region MFDs system

2.1 Dynamic equations and problem formulation

A partitioned traffic network is schematically shown in Fig. 1. There are two regions, $i = 1, 2$, where each region has a well-defined MFD, e.g. a city is partitioned to two regions: the periphery of the center (1) and the city center (2). Let us denote $n_i(t)$ [veh] as the accumulation or the total number of vehicles in i at time t, $q_1(t)$ [veh/sec] as the exogenous traffic flow

demand generated in region 1 with destination to region 2 at time t, while $q_2(t)$ [veh/sec] as the endogenous traffic flow demand generated in region 2 with destination to region 2 at time t, $G_i(n_i(t))$ [veh/sec] as the exit flow of the MFD in i at $n_i(t)$, and $u(t)$ [-] as the perimeter control, where $0 \leq u(t) \leq 1$.

The dynamic equations of two-region MFDs system are

$$\frac{\mathrm{d}n_1(t)}{\mathrm{d}t} = q_1(t) - G_1(n_1(t)) \cdot u(t) \tag{1}$$

$$\frac{\mathrm{d}n_2(t)}{\mathrm{d}t} = q_2(t) + G_1(n_1(t)) \cdot u(t) - G_2(n_2(t)) \tag{2}$$

The criterion is to maximize the output of the traffic network, i.e. the number of vehicles that complete their trips and reach their destinations. For the defined demand in our two-region MFDs system, i.e. exogenous demand from region 1 to region 2 and endogenous demand from region 2 to region 2, there is only one destination which is region 2, hence the maximum number of vehicles reach their destination is defined as

$$\max \int_0^{t_\mathrm{f}} G_2(n_2(t))\mathrm{d}t \tag{3}$$

where t_f [sec] is the control time horizon.

For simplicity, it is assumed that the demands are constant with time, i.e. $q_i(t) = q_i$, $i = 1, 2$, then the *two-region MFDs control problem* is formulated as follows: given an initial and end state variables $n_{1,0},\ n_{2,0}$ and $n_{1,\mathrm{f}},\ n_{2,\mathrm{f}}$, respectively, and control time horizon $[0, t_f]$, find the optimal control policy that maximizes the number of vehicles reach their destination with the dynamic equations (1) and (2), i.e.

$$J = \max \int_0^{t_\mathrm{f}} G_2(n_2(t))\mathrm{d}t \tag{4}$$

subject to

$$\frac{\mathrm{d}n_1(t)}{\mathrm{d}t} = q_1 - G_1(n_1(t)) \cdot u(t) \tag{5}$$

$$\frac{\mathrm{d}n_2(t)}{\mathrm{d}t} = q_2 + G_1(n_1(t)) \cdot u(t) - G_2(n_2(t)) \tag{6}$$

$$n_1(0) = n_{1,0}\ ;\ n_2(0) = n_{2,0} \tag{7}$$

$$n_1(t_\mathrm{f}) = n_{1,\mathrm{f}}\ ;\ n_2(t_\mathrm{f}) = n_{2,\mathrm{f}} \tag{8}$$

$$u_{\min} \leq u(t) \leq u_{\max} \tag{9}$$

where $0 < u_{\min}$ and $u_{\max} < 1$ are a priori given lower and upper bounds, respectively. Note that the control time horizon t_f is assumed to be large enough to reach end state point.

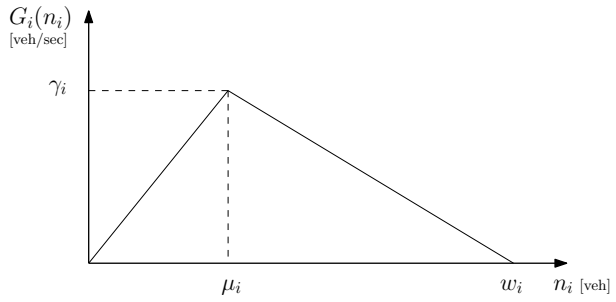

Figure 2: Triangle macroscopic fundamental diagram.

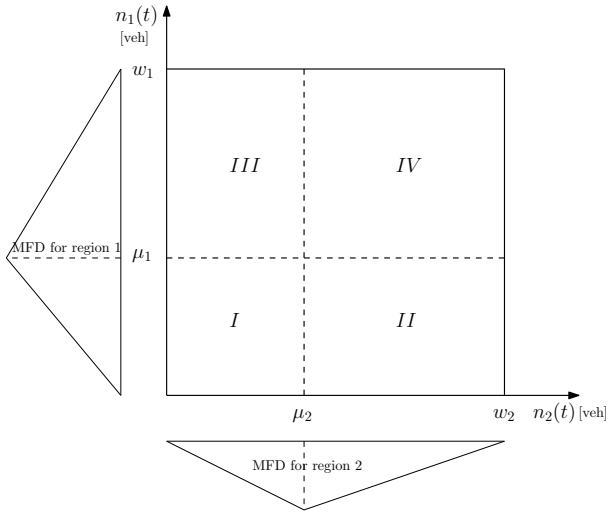

Figure 3: Four state regions in (n_2, n_1)-plane according to triangle MFDs.

The outputs of the two-region MFDs system are dependent on their shapes. In this paper, the MFDs for both the two regions, e.g. the city center and the periphery of the city, are assumed to be triangular, see Fig. 2, with capacity γ_i [veh/sec] at μ_i [veh], and jam density w_i [veh]. There are only two traffic regimes in the triangle shape: uncongested $0 \leq n_i(t) \leq \mu_i$ and congested $\mu_i \leq n_i(t) \leq w_i$. The triangle shape is defined as a piecewise affine function

$$G_i(n_i(t)) = \begin{cases} \frac{\gamma_i}{\mu_i} \cdot n_i(t) & \text{if } 0 \leq n_i(t) \leq \mu_i, \\ \frac{-\gamma_i}{w_i - \mu_i} \cdot n_i(t) + \frac{\gamma_i \cdot w_i}{w_i - \mu_i} & \text{if } \mu_i \leq n_i(t) \leq w_i, \end{cases} \tag{10}$$

Substituting (10) into the dynamic equations (5) and (6), one gets a piecewise second-order system of two state variables $n_1(t)$ and $n_2(t)$ with four *state regions*, see also Fig. 3:

- state region I, for $0 \leq n_1(t) \leq \mu_1$ and $0 \leq n_2(t) \leq \mu_2$,
- state region II, for $0 \leq n_1(t) \leq \mu_1$ and $\mu_2 \leq n_2(t) \leq w_2$,
- state region III, for $\mu_1 \leq n_1(t) \leq w_1$ and $0 \leq n_2(t) \leq \mu_2$,
- state region IV, for $\mu_1 \leq n_1(t) \leq w_1$ and $\mu_2 \leq n_2(t) \leq w_2$.

2.2 Phase portraits for piecewise second-order system

In order to investigate the behavior of the two states two-region MFDs system, a phase portraits is constructed by plotting trajectories from a large number of initial states spread all over the (n_2, n_1)-plane. The *qualitative behavior* of the trajectories near equilibrium points can be also determined via linearization with respect to these points, see Khalil (2002).

The equilibrium points, i.e. $\mathrm{d}n_i/\mathrm{d}t = 0$, $i = 1, 2$, in state regions I, II, III, and IV, according to the corresponding equations after substituting (10) into (5) and (6):

$$(n_{2,\mathrm{eq}}, n_{1,\mathrm{eq}})_I = \left(\frac{(q_1 + q_2) \cdot \mu_2}{\gamma_2} \, , \, \frac{q_1 \cdot \mu_1}{\gamma_1 \cdot u(t)} \right) \tag{11}$$

$$(n_{2,\mathrm{eq}}, n_{1,\mathrm{eq}})_{II} = \left(w_2 - \frac{(w_2 - \mu_2) \cdot (q_1 + q_2)}{\gamma_2} \, , \, \frac{q_1 \cdot \mu_1}{\gamma_1 \cdot u(t)} \right) \tag{12}$$

$$(n_{2,\mathrm{eq}}, n_{1,\mathrm{eq}})_{III} = \left(\frac{(q_1 + q_2) \cdot \mu_2}{\gamma_2} \, , \, w_1 - \frac{q_1 \cdot (w_1 - \mu_1)}{\gamma_1 \cdot u(t)} \right) \tag{13}$$

$$(n_{2,\mathrm{eq}}, n_{1,\mathrm{eq}})_{IV} = \left(w_2 - \frac{(w_2 - \mu_2) \cdot (q_1 + q_2)}{\gamma_2} \, , \, w_1 - \frac{q_1 \cdot (w_1 - \mu_1)}{\gamma_1 \cdot u(t)} \right) \tag{14}$$

Proposition 1. *The necessary and sufficient conditions for equilibrium points, i.e.* $\mathrm{d}n_i/\mathrm{d}t = 0$*,* $i = 1, 2$*, in state regions I, II, III, and IV of the two-region MFDs system with triangle shapes are:*

$$q_1 + q_2 < \gamma_2 \tag{15}$$

$$q_1 < \gamma_1 \cdot u(t) \tag{16}$$

Proof. If $\mathrm{d}n_i/\mathrm{d}t = 0$ for $i = 1, 2$ hold, then they imply (11)–(14), and by definition the equilibrium points in state region I, II, III, and IV, i.e. $(n_{2,\mathrm{eq}}, n_{1,\mathrm{eq}})_I$, $(n_{2,\mathrm{eq}}, n_{1,\mathrm{eq}})_{II}$, $(n_{2,\mathrm{eq}}, n_{1,\mathrm{eq}})_{III}$, and $(n_{2,\mathrm{eq}}, n_{1,\mathrm{eq}})_{IV}$ satisfy the lower and upper bounds of its region, i.e. $0 \leq n_1(t) \leq \mu_1$ and $0 \leq n_2(t) \leq \mu_2$ for state region I, $0 \leq n_1(t) \leq \mu_1$ and $\mu_2 \leq n_2(t) \leq w_2$ for state region II, $\mu_1 \leq n_1(t) \leq w_1$ and $0 \leq n_2(t) \leq \mu_2$ for state region III, and $\mu_1 \leq n_1(t) \leq w_1$ and $\mu_2 \leq n_2(t) \leq w_2$ for state region IV. Substituting each equilibrium point in the lower and upper bounds for its state region, one gets (15) and (16).

Clearly, if (15) and (16) hold, then each equilibrium point satisfies the lower and upper bounds for its region, i.e. there exist equilibrium points (11), (12), (13), and (14) such that they belong to state regions I, II, III, and IV, respectively. □

Let us rewrite (5) and (6), respectively, as

$$\frac{\mathrm{d}n_1(t)}{\mathrm{d}t} = f_1(n_1, n_2) \tag{17}$$

$$\frac{\mathrm{d}n_2(t)}{\mathrm{d}t} = f_2(n_1, n_2) \tag{18}$$

where $f_1(n_1, n_2) = q_1 - G_1(n_1(t)) \cdot u(t)$, $f_2(n_1, n_2) = q_2 + G_1(n_1(t)) \cdot u(t) - G_2(n_2(t))$. Let us assume that there exists at least one equilibrium point, denoted by $(n_{1,\mathrm{eq}}, n_{2,\mathrm{eq}})$, for (17) and (18), i.e. $\mathrm{d}n_i/\mathrm{d}t = 0$, $i = 1, 2$, then the Jacobian matrix of (17) and (18) at $n_{1,\mathrm{eq}}$, $n_{2,\mathrm{eq}}$

$$A = \left[\begin{array}{cc} \frac{\partial f_1}{\partial n_1} & \frac{\partial f_1}{\partial n_2} \\ \frac{\partial f_2}{\partial n_1} & \frac{\partial f_2}{\partial n_2} \end{array}\right] \Bigg|_{n_1=n_{1,\mathrm{eq}}, n_2=n_{2,\mathrm{eq}}} \tag{19}$$

Hence, under the assumption that (15) and (16) hold and for a given $u(t)$, one can calculate the Jacobian matrix at the equilibrium points in the state regions I, II, III, and IV according to

$$\begin{aligned} A_I &= \left[\begin{array}{cc} -\frac{\gamma_1}{\mu_1} \cdot u(t) & 0 \\ \frac{\gamma_1}{\mu_1} \cdot u(t) & -\frac{\gamma_2}{\mu_2} \end{array}\right] \qquad A_{II} = \left[\begin{array}{cc} -\frac{\gamma_1}{\mu_1} \cdot u(t) & 0 \\ \frac{\gamma_1}{\mu_1} \cdot u(t) & \frac{\gamma_2}{w_2-\mu_2} \end{array}\right] \\ A_{III} &= \left[\begin{array}{cc} \frac{\gamma_1}{w_1-\mu_1} \cdot u(t) & 0 \\ -\frac{\gamma_1}{w_1-\mu_1} \cdot u(t) & -\frac{\gamma_2}{\mu_2} \end{array}\right] \qquad A_{IV} = \left[\begin{array}{cc} \frac{\gamma_1}{w_1-\mu_1} \cdot u(t) & 0 \\ -\frac{\gamma_1}{w_1-\mu_1} \cdot u(t) & \frac{\gamma_2}{w_2-\mu_2} \end{array}\right] \end{aligned} \tag{20}$$

The type of the equilibrium points is determined according to the eigenvalues of matrices A_I, A_{II}, A_{III}, and A_{IV} in (20), see Khalil (2002). All these matrices are lower triangular matrices, hence, the eigenvalues are the elements in the triangle. The equilibrium point in region I is a *stable equilibrium node* since the two eigenvalues are negative, i.e. $-\gamma_1/\mu_1 \cdot u(t) < 0$ and $-\gamma_2/\mu_2 < 0$, the equilibrium points in region II and III are *unstable saddle points* since there are one positive and one negative eigenvalues: for region II the eigenvalues are $-\gamma_1/\mu_1 \cdot u(t) < 0$ and $\gamma_2/(w_2 - \mu_2) > 0$ while for region III the eigenvalues are $\gamma_1/(w_1 - \mu_1) \cdot u(t) > 0$ and $-\gamma_2/\mu_2 < 0$, and the equilibrium point in region IV is an *unstable node* since both eigenvalues are real positive, i.e. $\gamma_1/(w_1-\mu_1) \cdot u(t) > 0$ and $\gamma_2/(w_2-\mu_2) > 0$. The type of the equilibrium points are shown schematically in Fig. 4.

The phase portraits is numerically constructed according to the following steps under the assumption that the necessary and sufficient conditions (15) and (16) hold and that $u(t) = u$ is constant and a priori given during the construction of the phase portraits,

1. calculate all equilibrium points according to (11), (12), (13), and (14).

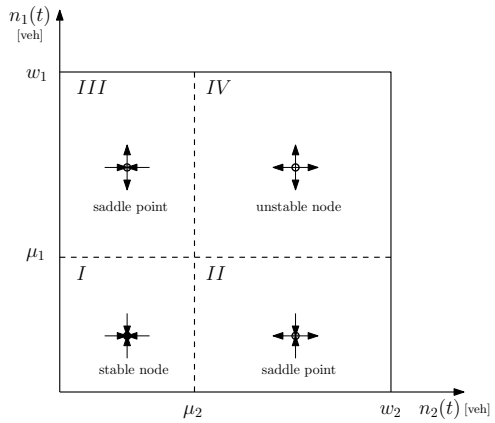

Figure 4: The type of equilibrium points in state regions I, II, III, and IV.

2. select a bounding box in the (n_2, n_1)-plane as

$$0 \leq n_1(t) \leq w_1 \tag{21}$$

$$0 \leq n_2(t) \leq w_2 \tag{22}$$

3. calculate trajectories[1] for selected initial points: inside and near the bounding box (21) and (22), and near calculated equilibrium points in step 1.

Following these steps, the phase portraits is numerically conducted for example 1 as shown in Fig. 5, where the green lines are the trajectories and the gray arrows are the direction of the trajectories. The input data for example 1 are as follows: the traffic flow demand rates are $q_1 = 0.194\,[\text{veh/sec}]$, $q_2 = 0.069\,[\text{veh/sec}]$, the perimeter control $u(t) = u_{\max} = 0.8$, the MFD parameters are: $\gamma_1 = 0.5\,[\text{veh/sec}]$, $\mu_1 = 50\,[\text{veh}]$, $w_1 = 200\,[\text{veh}]$, $\gamma_2 = 0.583\,[\text{veh/sec}]$, $\mu_2 = 150\,[\text{veh}]$, $w_2 = 450\,[\text{veh}]$.

3 Stability characterization of two states two-region system

The phase portrait conducted in the previous section shows that some of the trajectories reach an equilibrium point while other trajectories reach one (at least) jam density, e.g. see Fig. 5. Hence, before solving the two-region MFDs control problem, behavior and stability analysis of the two-region system are conducted.

According to Section 2.2, if the necessary and sufficient conditions (15) and (16) hold, then one stable equilibrium point exists in state region I. *Stable trajectories* are defined as trajectories that approach a stable equilibrium point in state region I $(n_{2,\text{eq}}, n_{1,\text{eq}})_I$ corresponding to $u(t)$

[1]Computer programs for solving ordinary differential equations are widely available. In this paper, Simulink the simulation tool of MATLAB is used.

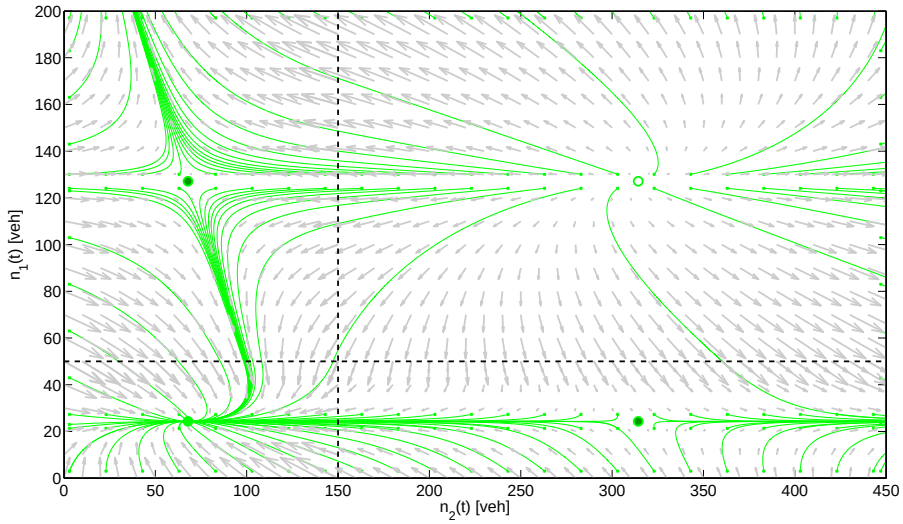

Figure 5: Phase portraits for numerical example 1.

as $t \to t_{\mathrm{f}}$, see (11), while *unstable trajectories* approach (at least) one jam density, i.e. $n_1(t_{\mathrm{f}}) = w_1$ or/and $n_2(t_{\mathrm{f}}) = w_2$, and there exists no control $u(t)$ that can bring trajectories to stable equilibrium point under the prevailing traffic demand. Moreover, a *stable region* is defined as the set of all points that have stable trajectories, while all other points with unstable trajectories define an *unstable region*.

A *region of attraction* for constant control $u(t) = u$, denotes by RA_u, is defined as the set of all points (n_2, n_1) that their trajectories are stable with applied control u. Finding the region of attraction of a nonlinear system is a significant research topic that has been studied extensively, e.g. Chiang and Thorp (1989); Mhaskar *et al.* (2006); Tan and Packard (2008); Topcu and Packard (2009). Since computing the exact RA is hard, researchers have focused on finding Lyapunov functions whose sublevel sets provide invariant subsets of the RA. There is no general Lyapunov function that may apply for nonlinear systems, therefore, different methods were presented for specific class of nonlinear systems, e.g. piecewise quadratic Lyapunov functions and linear matrix inequalities approach have been proposed in Hassibi and Boyd (1998) and Johansson and Rantzer (1998) for piecewise affine systems. It is a hard task to find a Lyapunov function for *bilinear systems*, which is a class of nonlinear control systems where the control u is act as an additive and multiplicative coefficient of state variables, Elliott (2009). Moreover, it was concluded in Gutman (1981) that there exists no general method to design stabilizing controllers for bilinear system. The two states two-region system is even more sophisticated than bilinear system since it is a *piecewise bilinear system*, however, a new algorithm is proposed to calculate the region of attraction according to analytical and numerical computations. RAs are used to characterize the stable and unstable regions in this section, and to design a state-feedback control in Section 4.

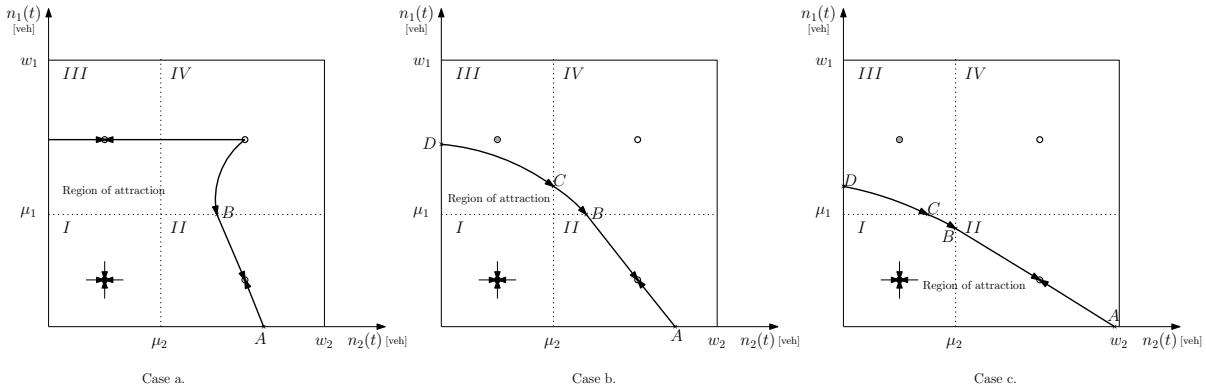

Figure 6: Region of attraction corresponding to constant control u: cases a, b, and c

3.1 Region of attraction boundary

Since the two-region MFDs system is piecewise system, and has an equilibrium point in each piece, three different cases are distinguished. In case a, the equilibrium points in state regions III and IV are "far" enough from each other such that trajectories do not interfere each other, therefore, the type of equilibrium points and the qualitative behavior near them are maintained as two isolated points in the state space, see Fig. 4. In case b and c, the two equilibrium points in region II and III affect each other, hence, the behavior of trajectories is different than that in case a. The region of attraction boundaries for constant control for cases a, b, and c are schematically shown in Fig. 6.

Under the assumption that $u(t)$ is constant during the control time horizon, i.e. $u(t) = u$ for $[0, t_f]$, the following steps are presented for computing the RA boundary curve, see Fig. 6:

1. calculate all equilibrium points according to (11), (12), (13), and (14).

2. start from the saddle equilibrium point in state region II, and calculate the corresponding eigenvector of the negative eigenvalue of the linearized system in that region, i.e. $\lambda_1 = -\gamma_1/\mu_1 \cdot u < 0$, according to

$$(n_2, n_1) = \left(1, \frac{-\gamma_2 \cdot \mu_1}{\gamma_1 \cdot u \cdot (w_2 - \mu_2)} - 1\right) \tag{23}$$

   therefore, the slope of line AB is $-\gamma_2 \cdot \mu_1/(\gamma_1 \cdot u \cdot (w_2 - \mu_2)) - 1$.

3. given the slope of the line AB and the saddle equilibrium point $(n_{2,\text{eq}}, n_{1,\text{eq}})_{II}$, calculate points $A = (n_{2,A}, n_{1,A})$ and $B = (n_{2,B}, n_{1,B})$, and draw line AB, where point A is the intersection between line AB and line $n_1(t) = 0$ or line $n_2(t) = w_2$, and point B is the intersection between line AB and line $n_1(t) = \mu_1$ or line $n_2(t) = \mu_2$, depending on the value of the slope.

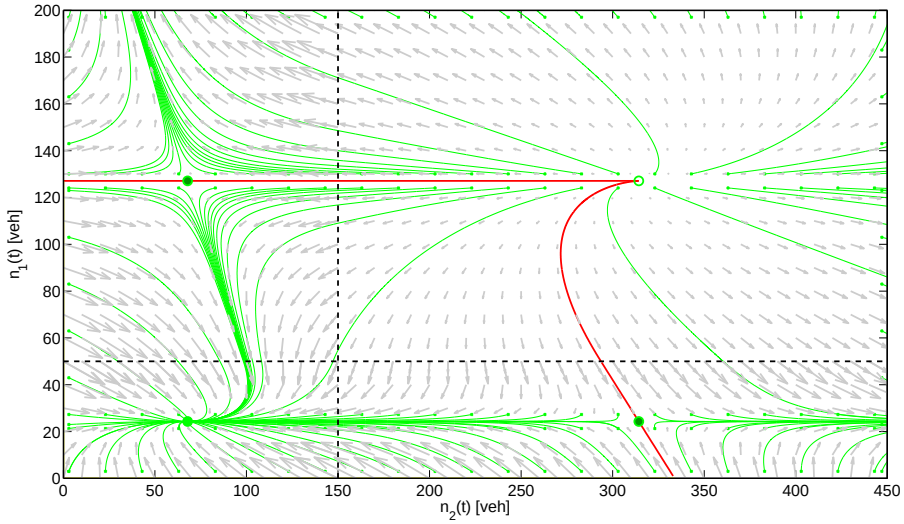

Figure 7: Numerical example 1 demonstrates case a: the trajectories are in green and the red curve is the boundary.

4. if $n_{2,B} > \mu_2$, then calculate trajectory from point B to the unstable equilibrium point $(n_{2,\text{eq}}, n_{1,\text{eq}})_{IV}$ in reverse direction according to (47), (48), and (49) in A.1, with initial state point B and $t = 0 \to \infty$. If the trajectory B-$(n_{2,\text{eq}}, n_{1,\text{eq}})_{IV}$ does not enter the state region III, i.e. does not intersect the line $n_2(t) = \mu_2$, then it is case a, otherwise it is case b:

   - case a: draw a horizontal line stars from the unstable equilibrium point $(n_{2,\text{eq}}, n_{1,\text{eq}})_{IV}$ moves through the saddle point $(n_{2,\text{eq}}, n_{1,\text{eq}})_{III}$, and ends at $n_2(t) = 0$. The line is horizontal according to the corresponding eigenvector of the negative eigenvalue for the saddle equilibrium point in state region III.
   - case b: calculate trajectories from points B to C and C to D in reverse way, according to A.2.

5. if $n_{2,B} = \mu_2$ then it is case c. Calculate trajectory from points B to C and C to D in reverse way according to A.3.

Note that the RA boundary curve is combined from several trajectories some of them are calculated numerically, while other trajectories are calculated analytically, see A.1, A.2, and A.3.

The region of attraction boundaries for cases a, b, and c are demonstrated by examples 1, 2, and 3, as shown in Fig. 7, 8, and 9, respectively, where the red curve is the RA boundary. The input data for example 1 are given in Section 2.2. The input data for example 2 are as follows: the traffic flow demand rates are $q_1 = 0.194\,[\text{veh/sec}]$, $q_2 = 0.319\,[\text{veh/sec}]$, the perimeter control $u(t) = u_{\max} = 0.8$, the MFD parameters are: $\gamma_1 = 0.5\,[\text{veh/sec}]$, $\mu_1 = 50\,[\text{veh}]$, $w_1 = 200\,[\text{veh}]$, $\gamma_2 = 0.583\,[\text{veh/sec}]$, $\mu_2 = 150\,[\text{veh}]$, $w_2 = 450\,[\text{veh}]$. The input data for example 3 are as follows: the traffic flow demand rates are $q_1 = 0.194\,[\text{veh/sec}]$, $q_2 = 0.278\,[\text{veh/sec}]$,

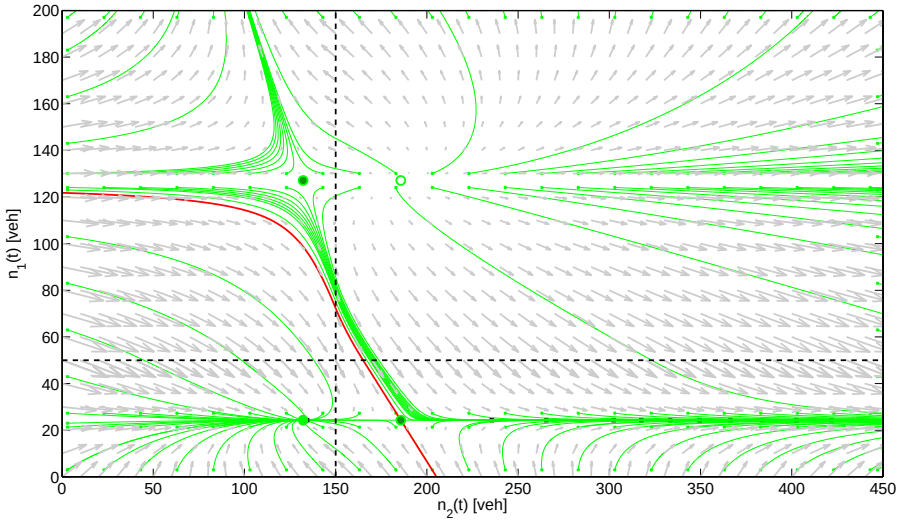

Figure 8: Numerical example 2 demonstrates case b: the trajectories are in green and the red curve is the boundary.

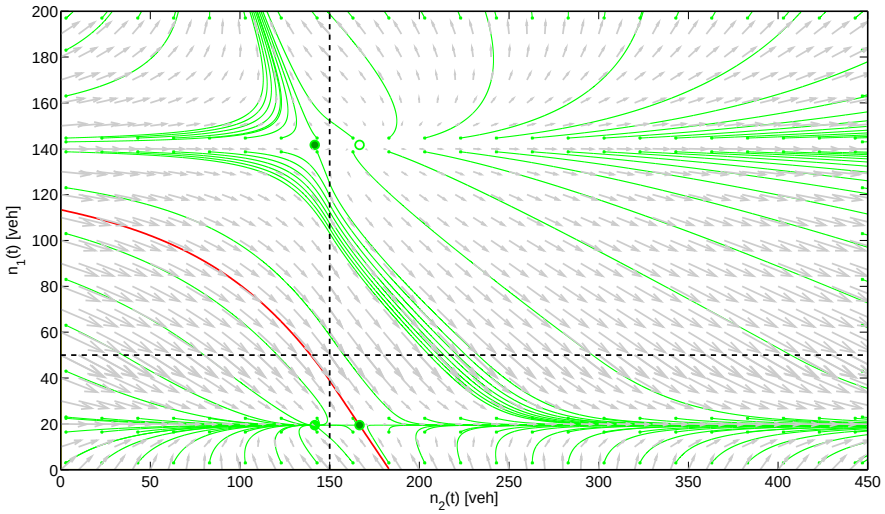

Figure 9: Numerical example 3 demonstrates case c: the trajectories are in green and the red curve is the boundary.

the perimeter control $u(t) = u_{\max} = 1$, the MFD parameters are: $\gamma_1 = 0.5\,[\text{veh/sec}]$, $\mu_1 = 50\,[\text{veh}]$, $w_1 = 200\,[\text{veh}]$, $\gamma_2 = 0.5\,[\text{veh/sec}]$, $\mu_2 = 150\,[\text{veh}]$, $w_2 = 450\,[\text{veh}]$.

Until this section, the RA boundaries for all numerical examples 1, 2, and 3 were calculated for constant control $u(t) = u_{\max}$ (trajectories drawn by green color). Clearly, different RA boundaries and trajectories are obtained by applying $u(t) = u_{\min}$, e.g. the phase portraits with the RA for example 1 corresponding to $u(t) = u_{\min} = 0.45$ and $u(t) = u_{\max}$ are shown in Fig. 10, where trajectories are drawn by blue color and the boundary by cyan color for $u_{\min}$.

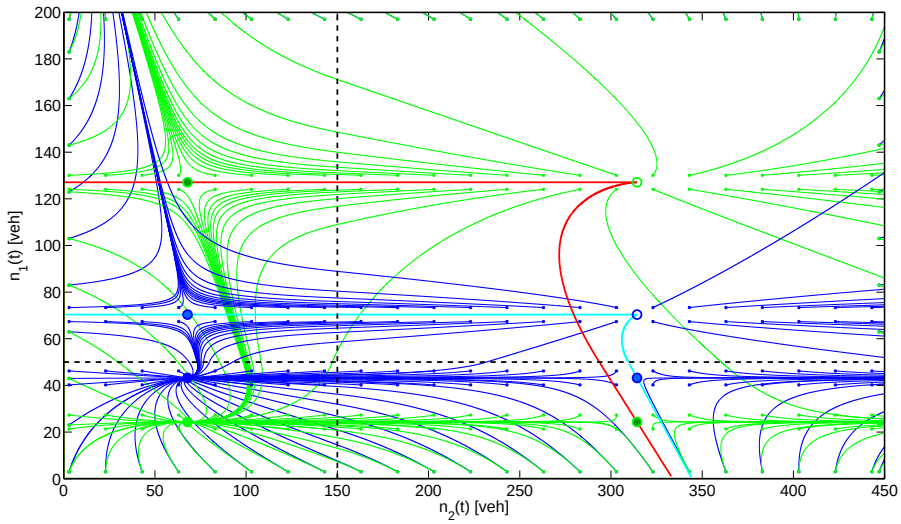

Figure 10: Numerical example 1 corresponding to $u(t) = u_{\min}$ (trajectories in blue and RA boundary in cyan) and $u(t) = u_{\max}$ (trajectories in green and RA boundary in red).

3.2 Stability characterization

In the previous section, an algorithm is proposed to compute the RA_u boundary for a constant control u. In this section, the algorithm for computing the RA is used to characterize the stable and unstable regions.

Recall that stable region is defined as the set of all points that have (at least) one trajectory approaches a stable equilibrium point corresponding to control $u(t)$. If $u(t)$ is assumed to be constant for the whole control period, then the stable region is the set of all possible RAs. However, since the control may change over the control period, the stable region is wider, i.e. points outside the set of all RAs may also be stable if there exits (at least) one trajectory that enters the set of all RAs region.

In principle, in order to characterize the stable region, one has to calculate RAs corresponding to all u satisfies (9) and explore the state space for trajectories that enter these RAs. However, qualitative behavior and numerical examples, e.g. Fig.11, show that computations of $\mathrm{RA}_{u_{\min}}$ and a few trajectories are enough to characterize the stable region boundary. The quantitative behavior of RAs for a wide range of u are shown in Fig.11 for numerical example 4 where its input data are the same of example 1 except $q_2(t) = 0.347\,[\mathrm{veh/sec}]$ instead of $q_2(t) = 0.07\,[\mathrm{veh/sec}]$.

From the qualitative behavior of the RAs shown in Fig. 6, two stable regions are distinguished according to $\mathrm{RA}_{u_{\min}}$, see also Fig. 12:

- Case i: $\mathrm{RA}_{u_{\min}}$ belong to case a,
- Case ii: $\mathrm{RA}_{u_{\min}}$ belongs to case b or case c.

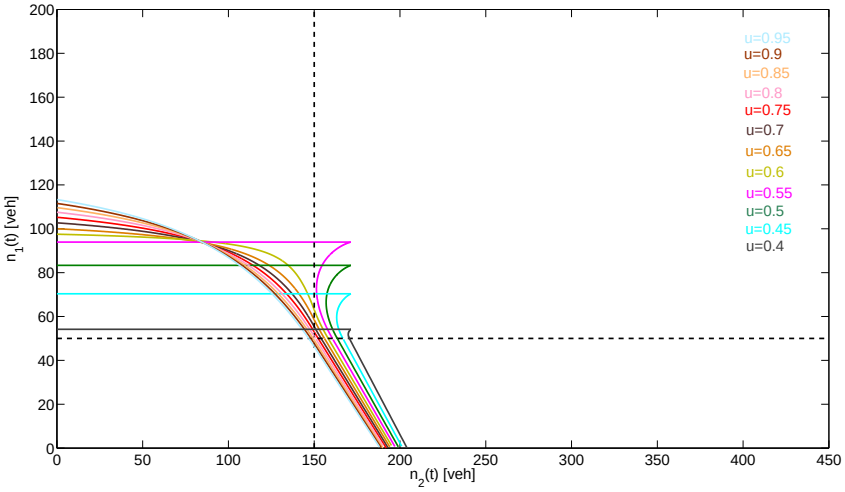

Figure 11: Example 4: RAs for wide range of u

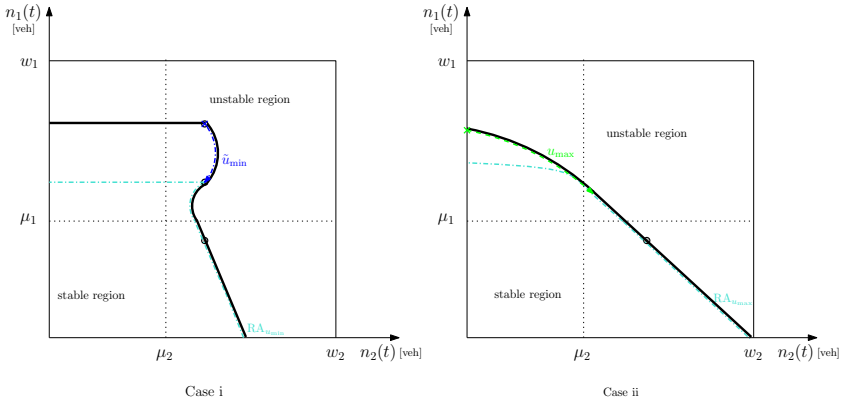

Figure 12: Stable and unstable regions cases i and ii

The solid curve in Fig. 12 is a boundary that splits (n_2, n_1)-plane into stable and unstable regions, i.e. stability characterization needs $\mathrm{RA}_{u_{\min}}$, and one numerical trajectory which can be found numerically: for cases i reverse trajectory calculation with $u_{\min}$, denoted by $\tilde{u}_{\min}$, starts from unstable equilibrium point in state region IV according to $u_{\max}$ and for case ii trajectory starts from the horizontal axes with $u_{\max}$ and tangent with $\mathrm{RA}_{u_{\min}}$, see Fig. 12. Numerical example 4 with different upper and lower bounds $u_{\max}$, $u_{\min}$ demonstrates cases i and ii as shown in Fig. 13 and Fig. 14, respectively.

In Section 3.1, the RA boundary was analyzed for dynamics equations with constant demand q_1 and q_2, see (5) and (6). However, the same analysis can be also used for time varying demand $q_1(t)$ and $q_2(t)$, see (1) and (2), since for these dynamics equations (1) and (2) no bifurcation happens, i.e. the difference in behavior around equilibrium points is quantitative but not qualitative when demand varies, it means that there will be one stable and unstable equilibrium points in state regions I and IV, respectively, two saddle equilibrium points in regions II and III, and only the positions of the equilibria points varies within each region. The reason that no bifurcation happens with time varying demand is that each equilibrium point is a function of $q_1(t)$

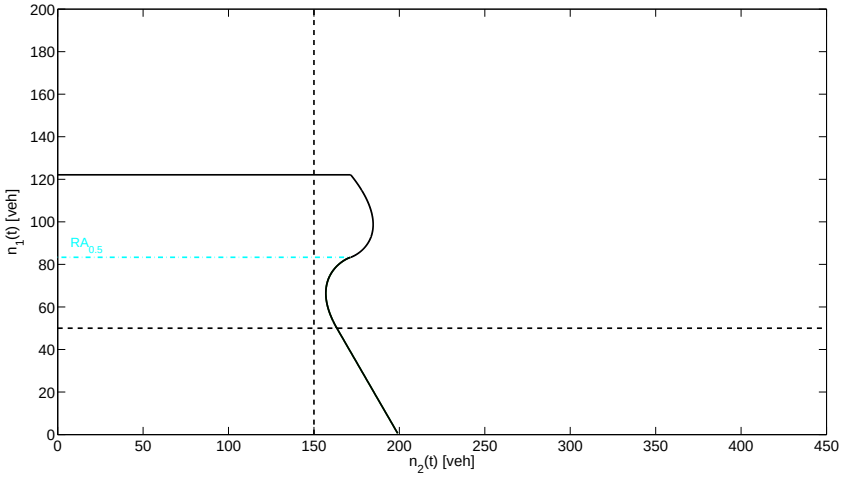

Figure 13: Example 4 with $u_{\max} = 0.75$ and $u_{\min} = 0.5$ demonstrates stable and unstable regions for case i

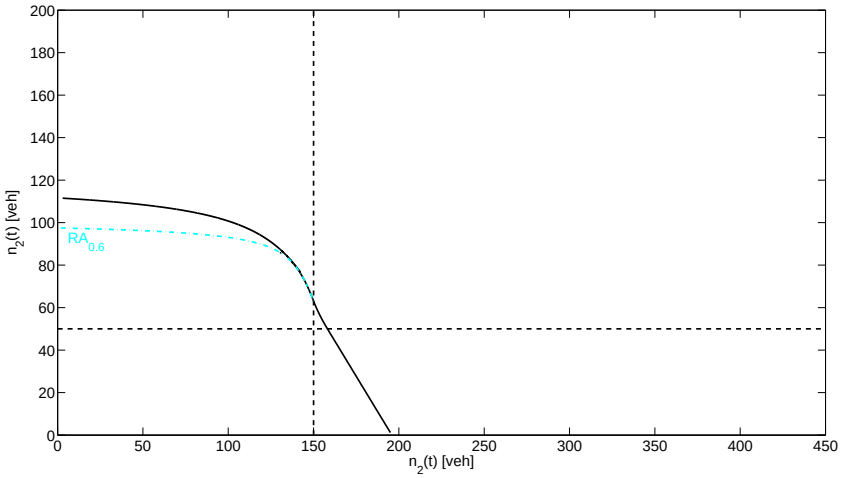

Figure 14: Example 4 with $u_{\max} = 0.75$ and $u_{\min} = 0.6$ demonstrates stable and unstable regions for case ii

and $q_2(t)$, i.e. $n_{1,\text{eq}}(q_1(t), q_2(t))$, $n_{2,\text{eq}}(q_1(t), q_2(t))$. Then, $n_{1,\text{eq}}(q_1(t), q_2(t))$, $n_{2,\text{eq}}(q_1(t), q_2(t))$ is a smooth function of $q_1(t)$, $q_2(t)$, as long as the Jacobian linearization around equilibrium points does not have a zero eigenvalue, see Izhikevich (2007); Khalil (2002), and this holds in our case since the demand is an affine parameter of the system.

In example 1, the exogenous demand from the periphery of the center to the city center is $q_1 = 0.194$ [veh/sec], while the endogenous demand from and to the city center is $q_2 = 0.069$ [veh/sec]. Examples 2 and 3 show the effect of different demand q_2 and q_1, respectively. In example 2, the effect of different endogenous demand $q_2 = 0.069, 0.125, 0.181, 0.236$,0.292, 0.347 [veh/sec] with $q_1 = 0.194$ [veh/sec], $u_{\max} = 0.8$ and $u_{\min} = 0.45$ on the stable and unstable regions is shown in Fig. 15, while in example 3, the effect of different exogenous demand $q_1 = 0.083$, 0.111, 0.138, 0.166 , 0.194, 0.222 [veh/sec] with $q_2 = 0.181$ [veh/sec], $u_{\max} = 0.8$ and $u_{\min} = 0.45$ on the stable and unstable regions is shown in Fig. 16. Results in

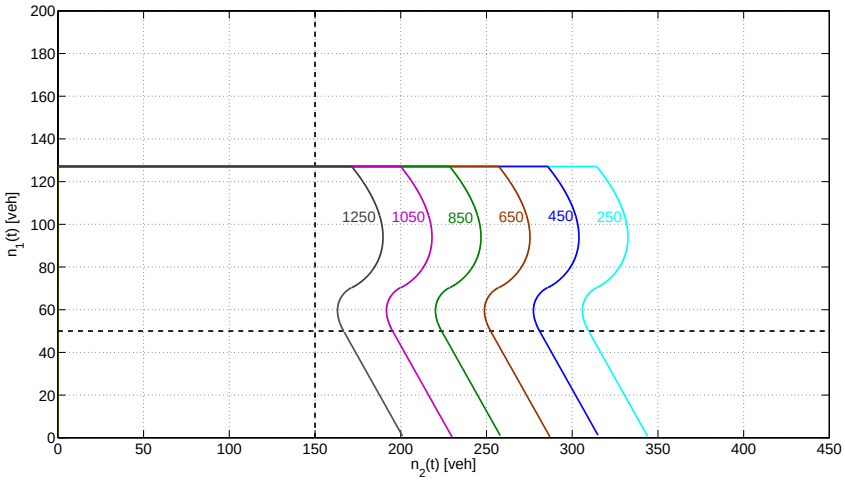

Figure 15: Numerical example 2: stable regions for different q_2 demand.

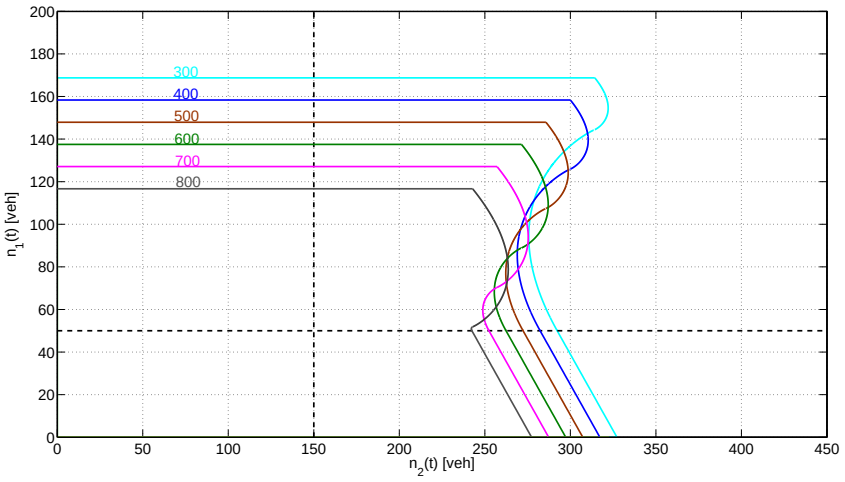

Figure 16: Numerical example 3: stable regions for different q_1 demand.

Fig. 15 and Fig. 16 are as expected. The stable region becomes smaller as demand increases, since increasing demand q_2 or/and demand q_1 increases the destination to region 2 which becomes more congested, then the system of the two regions will intend to be jammed, i.e. larger unstable region and smaller stable region.

4 State-feedback control for two-region MFDs

In this section, the stabilizing control solution is derived for the two-region MFDs control problem (4)–(9). It will be shown in Section 4.1 that the two-region control problem is a feasibility (or stabilizing) problem, i.e. any feasible sequence of perimeter control is an optimal solution, and all feasible solutions have the same value of the criterion for the same initial and end states. However, when the control problem has no feasible solution for the initial state, then the control cannot stabilize the two-region MFDs and the stable equilibrium end point is not

reachable, hence, an optimal solution is derived for a relaxed problem as shown in Section 4.2.

4.1 Stabilizing control for feasibility control problem

First, let us assume that the two-region MFDs control problem has a feasible solution for the given initial state, i.e. one (at least) feasible solution $u(t)$ exists for $0 \leq t \leq t_f$, such that satisfies (9) and can bring initial states (7) to end states (8) in time duration t_f according to (5) and (6). In this case, one can integrate the differential equations (5) and (6), respectively,

$$n_{1,\mathrm{f}} = \int_0^{t_\mathrm{f}} q_1 \mathrm{d}t - \int_0^{t_\mathrm{f}} G_1(n_1(t)) \cdot u(t) \mathrm{d}t + n_{1,0} \tag{24}$$

$$n_{2,\mathrm{f}} = \int_0^{t_\mathrm{f}} q_2 \mathrm{d}t + \int_0^{t_\mathrm{f}} G_1(n_1(t)) \cdot u(t) \mathrm{d}t - \int_0^{t_\mathrm{f}} G_2(n_2(t)) \mathrm{d}t + n_{2,0} \tag{25}$$

then the two equations (24) and (25) are summed, one gets

$$n_{1,\mathrm{f}} + n_{2,\mathrm{f}} = \int_0^{t_\mathrm{f}} (q_1 + q_2) \mathrm{d}t - \int_0^{t_\mathrm{f}} G_2(n_2(t)) \mathrm{d}t + n_{1,0} + n_{2,0} \tag{26}$$

Note that $\int_0^{t_\mathrm{f}} G_2(n_2(t)) \mathrm{d}t$ is the criterion to be optimized, see (4), hence substituting (4) into (26), one gets

$$J = \max_u \Big(- n_{1,\mathrm{f}} - n_{2,\mathrm{f}} + \int_0^{t_\mathrm{f}} (q_1 + q_2) \mathrm{d}t + n_{1,0} + n_{2,0} \Big) \tag{27}$$

which is equivalent to optimize:

$$J = \min_u \Big(n_{1,\mathrm{f}} + n_{2,\mathrm{f}} \Big) \tag{28}$$

Hence, (28) implies (4). When the end state is a priori known, then the criterion J is *independent* of $u(t)$ and the problem is a feasibility control problem: if any applied control $u(t)$ brings the initial state $(n_{2,0}, n_{1,0})$ to the end state $(n_{2,\mathrm{f}}, n_{1,\mathrm{f}})$ in time duration t_f where the initial state, end state, and t_f are a priori known, then the applied control $u(t)$ is optimal, in other words, all feasible controllers are also optimal. However, when the end point is assumed to be a stable equilibrium point in stable region I, then according to (11) the sum of end state $n_{1,\mathrm{f}} + n_{2,\mathrm{f}}$ (28) is minimized when the control sequence ends with $u(t_\mathrm{f}) = u_{\max}$.

Note that (27) is generally derived for any trajectory that moves and stays in the same region, i.e. $G_1(n_1(t))$ and $G_2(n_2(t))$ are the same functions for $0 \leq t \leq t_f$. However, it is easily shown that (27) holds also for trajectory that moves from one region to another while reaching the end state point. For example, let us consider a trajectory that moves through three state regions IV, III, and I, as shown in Fig. 17, where t_1 and t_2 the time instants when trajectory

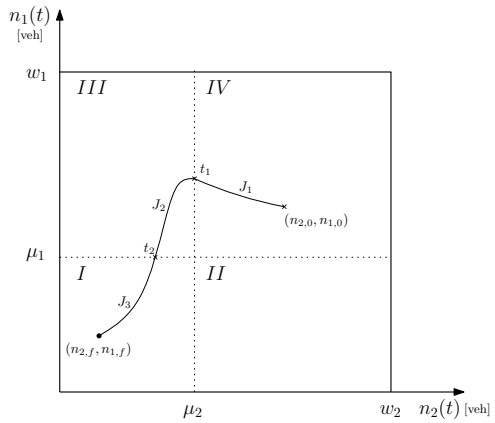

Figure 17: Trajectory moves through three regions IV, III, and I

enters state region III and I, respectively. One can calculate the value of the criterion J_1 in region IV for $[0, t_1]$, and J_2 in region III for $[t_1, t_2]$, and J_3 in region I for $[t_2, t_f]$ according to (27), respectively,

$$J_1 = -n_1(t_1) - n_2(t_1) + \int_0^{t_1} (q_1 + q_2)\mathrm{d}t + n_{1,0} + n_{2,0} \tag{29}$$

$$J_2 = -n_1(t_2) - n_2(t_2) + \int_{t_1}^{t_2} (q_1 + q_2)\mathrm{d}t + n_1(t_1) + n_2(t_1) \tag{30}$$

$$J_3 = -n_{1,\mathrm{f}} - n_{2,\mathrm{f}} + \int_{t_2}^{t_f} (q_1 + q_2)\mathrm{d}t + n_1(t_2) + n_2(t_2) \tag{31}$$

The value of the criterion J from 0 to t_f is calculated by summation of J_1 (29), J_2 (30), and J_3 (31), one gets (27). Hence, (27) holds for any trajectory that moves through different regions with different $G_1(n_1(t))$ and $G_2(n_2(t))$, and the problem is still a feasibility problem. Note that according to (27), the control problem is still a feasibility problem when demand varies with time. Instead of constant demand inside the integral, it will be substituted by time varying demand, which does not affect the derivation of (27).

However, the control problem may be not feasible for all initial states where the end state is not reachable, hence an optimal solution is derived for a relaxed problem where the end state is free.

4.2 Optimal control for relaxed control problem

When the two-region control problem (4)–(9) has no feasible solution for the initial state, an optimal solution is derived for a relaxed control problem: the two-region control problem with free end state, i.e. (4), (5), (6), (7), (9), and $(n_{2,\mathrm{f}}, n_{1,\mathrm{f}})$ is free. Note that for the relaxed problem, the assumption that control time horizon t_f is large enough to reach end state is dropped since the end state is free. The optimal relaxed control problems are solved separately for the 4

state regions in the (n_2, n_1)-plane corresponding to $G_i(n_i(t))$, $i = 1, 2$, in each state region. The Pontryagin maximum principe is used to solve the relaxed problems, see Pontryagin *et al.* (1962). In the following, the optimal solution is presented in details only for state region I.

For state region I, the *Hamiltonian*, denoted by H_I, is formed as

$$H_I = R_{1,\mathrm{I}} \cdot n_1(t) \cdot u(t) \cdot (p_2(t) - p_1(t)) + p_1(t) \cdot q_1 + p_2(t) \cdot (q_2 - R_{2,\mathrm{I}} \cdot n_2(t)) + R_{2,\mathrm{I}} \cdot n_2(t) \tag{32}$$

where $R_{1,\mathrm{I}} = \gamma_1/\mu_1$, $R_{2,\mathrm{I}} = \gamma_2/\mu_2$, and $p_1(t),\ p_2(t)$ are the *costate* variables that satisfy

$$\frac{\mathrm{d}p_1}{\mathrm{d}t} = -\frac{\partial H}{\partial n_1} = R_{1,\mathrm{I}} \cdot u(t) \cdot (p_1(t) - p_2(t)) \tag{33}$$

$$\frac{\mathrm{d}p_2}{\mathrm{d}t} = -\frac{\partial H}{\partial n_2} = R_{2,\mathrm{I}} \cdot (p_2(t) - 1) \tag{34}$$

Recall that the end state $(n_2(t_f), n_1(t_f))$ is free, hence according to Pontryagin *et al.* (1962) it follows that

$$p_1(t_f) = 0 \tag{35}$$

$$p_2(t_f) = 0 \tag{36}$$

The Hamiltonian must be maximized over the control variable $u(t)$ subject to the control constraint (9). The optimal control solution obtained by $\max_u H$ in (32) is

$$u(t) = \begin{cases} u_{\max} & \text{if } p_2(t) - p_1(t) > 0, \\ u_{\min} & \text{if } p_2(t) - p_1(t) < 0. \end{cases} \tag{37}$$

A *switching point* t_s [sec] is the time instant that satisfies $p_2(t_s) = p_1(t_s)$. If there exists a switching point, then the optimal policy will be determined by that point.

The initial conditions of the costates should be chosen such that the resulting solution satisfies the constraints (35), (36) and optimality condition (37). Note that if $p_2(0) > 1$ then $\mathrm{d}p_2/\mathrm{d}t > 0$, see (34), but this is a contradiction since $p_2(t_f) = 0$, see (36), hence lets assume that $p_2(t)$ is $0 \leq p_2(t) < 1$ and $p_1(0) > 0$. Since $p_1(t_f) = 0$, see (35), $p_1(t)$ must be decreasing for $0 \leq t < t_f$, i.e. $\mathrm{d}p_1/\mathrm{d}t < 0$, which implies $p_1(t) < p_2(t)$ for $0 \leq t < t_f$ according to (33), therefore the optimal control is $u(t) = u_{\max}$, see (37). In this case, there will be no switching point t_s otherwise $\mathrm{d}p_1/\mathrm{d}t > 0$ for $t_\mathrm{s} \leq t \leq t_f$, however $p_1(t_f) = 0$ is not satisfied, therefore $t_\mathrm{s} = t_f$.

The optimal solutions for the other three regions II, III, and IV are derived in a similar way, however the derivations and an independent check of optimality performed by numerical solu-

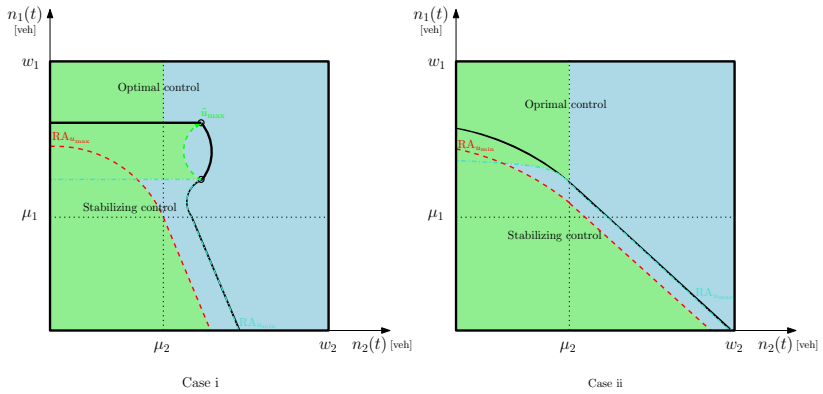

Figure 18: State-feedback control for cases i and ii (green: apply $u_{\max}$, blue: apply $u_{\min}$)

tions of the corresponding linear programming models of the four state regions are not shown here. The summary of optimal solutions for the relaxed problems is as follows, if the initial state $(n_{2,0}, n_{1,0})$ belongs to: state region I apply $u(t) = u_{\max}$, state region II apply $u(t) = u_{\min}$, state region III apply $u(t) = u_{\min}$, and state region IV apply $u(t) = u_{\min}$.

4.3 State-feedback control strategy

A state-feedback control strategy is proposed according to the feasibility of two-region control problem (4)–(9), see Fig. 18. If the control problem has a feasible solution for the initial state, i.e. the initial state belongs to the stable region, then a stabilizing state-feedback is applied to reach the optimal stable equilibrium point, otherwise, if the initial state belongs to the unstable region then an optimal state-feedback is applied, see Section 4.2.

The stabilizing state-feedback control depends on the $\mathrm{RA}_{u_{\max}}$, $\mathrm{RA}_{u_{\min}}$ for case ii and also on $\tilde{u}_{\max}$ for case i, where $\tilde{u}_{\max}$ is a reverse trajectory calculated with $u_{\max}$ starts from unstable equilibrium point in state region IV corresponding to $u_{\min}$, see Fig. 18. Note that it is not necessary that $\tilde{u}_{\max}$ trajectory ends in unstable equilibrium point corresponding to $u_{\max}$ as shown in the figure.

The stabilizing state-feedback control is as follows. If the initial state belongs to the $\mathrm{RA}_{u_{\max}}$, then apply $u(t) = u_{\max}$ for $0 \leq t \leq t_{\mathrm{f}}$ since it is proved that the value of the criterion is optimized with $u(t_{\mathrm{f}}) = u_{\max}$, see Section 4.1. If the initial state does not belong to $\mathrm{RA}_{u_{\max}}$ but belongs to the $\mathrm{RA}_{u_{\min}}$, then apply $u(t) = u_{\min}$ until the state trajectory enters the $\mathrm{RA}_{u_{\max}}$. If the initial state belongs to the stable region and does not belong to $\mathrm{RA}_{u_{\max}}$ or $\mathrm{RA}_{u_{\min}}$, then for case ii apply $u(t) = u_{\max}$, however, for case i it depends on $\tilde{u}_{\max}$ which splits this region to two: implement $u_{\max}$ for a point in region between $\mathrm{RA}_{u_{\max}}$ and $\tilde{u}_{\max}$, and apply $u_{\min}$ for region between $\tilde{u}_{\max}$ and the border of stable region, see Fig.18.

The state-feedback control strategy (n_2, n_1)-plane is demonstrated by example 4 with $u_{\max} =$

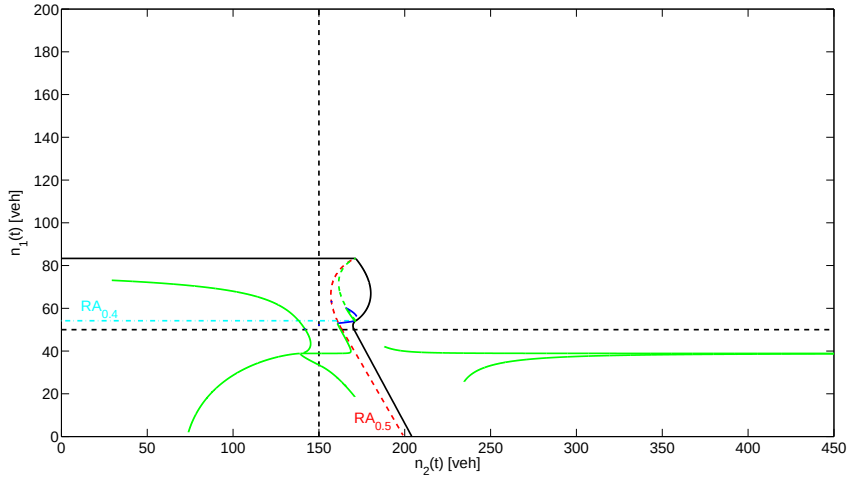

Figure 19: State-feedback control strategy for example 4.

0.5, $u_{\min} = 0.4$ for several initial state points, as shown in Fig. 19.

Note that when the demands are essentially non-constant the state-feedback control solution can be used in the scheme of a predictive control by recalculating boundary stable region, $\mathrm{RA}_{u_{\max}}$, $\mathrm{RA}_{u_{\min}}$, and control at each new control step where the time varying demands can be approximated as constant demands for each control step.

Remark 1. *If the necessary and sufficient conditions (15) and (16) for equilibrium points do not hold for the current demands, i.e. the system does not have a stable equilibrium point, the control problem (4)–(9) has no feasible solution for any $u(t)$ since the end point is defined as a stable equilibrium point. In this case, the optimal control solution is identical to the relaxed problems and should be applied until the demands change with time such that the necessary and sufficient conditions (15) and (16) hold.*

5 Region of attraction for three states two-region system

In the previous section, a state-feedback solution is derived for the two states two-region problem. It was shown that when the necessary and sufficient conditions (15) and (16) hold, then the state space of the control problem is divided to stable and unstable regions, where each region has different state-feedback control: a stabilizing for stable region and an optimizing for unstable regions. Recall that RAs were used in the two states two-region control for stability characterization and state feedback strategy.

This state-feedback strategy holds for more complicated two-region system, e.g. two regions with three demand. However, the characterization of a stable and unstable regions for three state system is a tedious task but straightforward. Hence, only numerical results for RAs for three states two-region system are presented.

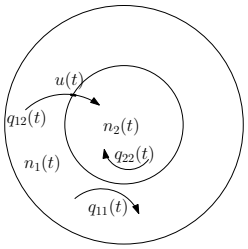

Figure 20: System of three states two-region system.

A partitioned traffic network with three demand is schematically shown in Fig. 20. There are two endogenous demand $q_{ii}(t)$ [veh/sec], $i = 1, 2$, and one exogenous demand $q_{12}(t)$ [veh/sec]. Therefore, three accumulation states $n_{11}(t)$, $n_{12}(t)$, and $n_2(t)$ [veh] are needed to model the dynamics equations, where $n_{11}(t)$ or $n_{12}(t)$ is the total number of vehicles in region (1) with destination (1) or (2) at time t, respectively, note that $n_1(t) = n_{11}(t) + n_{12}(t)$.

The control problem of three states two-region system is formulated as follows:

$$J = \max \int_0^{t_\mathrm{f}} \left[\frac{n_{11}(t)}{n_1(t)} \cdot G_1(n_1(t)) + G_2(n_2(t)) \right] \mathrm{d}t \tag{38}$$

subject to

$$\frac{\mathrm{d}n_{11}(t)}{\mathrm{d}t} = q_{11}(t) - \frac{n_{11}(t)}{n_{11}(t) + n_{12}(t)} \cdot G_1(n_1(t)) \tag{39}$$

$$\frac{\mathrm{d}n_{12}(t)}{\mathrm{d}t} = q_{12}(t) - \frac{n_{12}(t)}{n_{11}(t) + n_{12}(t)} \cdot G_1(n_1(t)) \cdot u(t) \tag{40}$$

$$\frac{\mathrm{d}n_2(t)}{\mathrm{d}t} = q_2(t) + \frac{n_{12}(t)}{n_{11}(t) + n_{12}(t)} \cdot G_1(n_1(t)) \cdot u(t) - G_2(n_2(t)) \tag{41}$$

$$n_{11}(0) = n_{11,0} \; ; \; n_{12}(0) = n_{12,0} \; ; n_2(0) = n_{2,0} \tag{42}$$

$$n_{11}(t_\mathrm{f}) = n_{11,\mathrm{f}} \; ; \; n_{12}(t_\mathrm{f}) = n_{12,\mathrm{f}} \; ; n_2(t_\mathrm{f}) = n_{2,\mathrm{f}} \tag{43}$$

$$u_{\min} \leq u(t) \leq u_{\max} \tag{44}$$

Note that the optimization control problem for the three accumulation states (38)–(44) is also a feasibility problem. This is easily proved in the same way as was done for the two states problem, see Section 4.1.

The input data for numerical example 5 are similar to example 1. However, the demand $q_1(t) = 0.194[\mathrm{veh/sec}]$ is split into two demands: $q_{11}(t) = 4/7 \cdot q_1(t) = 0.111[\mathrm{veh/sec}]$ and $q_{12}(t) = 3/7 \cdot q_1(t) = 0.083[\mathrm{veh/sec}]$. The boundary surfaces of $\mathrm{RA}_{u_{\max}}$ and $\mathrm{RA}_{u_{\min}}$ are shown in red and cyan color, respectively, in Fig. 21. The rest of the input data is as follows: the traffic flow demand rate $q_2 = 0.069\,[\mathrm{veh/sec}]$, the perimeter control $u_{\max} = 0.8$, $u_{\min} = 0.45$, the MFD parameters are: $\gamma_1 = 0.5\,[\mathrm{veh/sec}]$, $\mu_1 = 50\,[\mathrm{veh}]$, $w_1 = 200\,[\mathrm{veh}]$, $\gamma_2 = 0.583\,[\mathrm{veh/sec}]$, $\mu_2 = 150\,[\mathrm{veh}]$, $w_2 = 450\,[\mathrm{veh}]$.

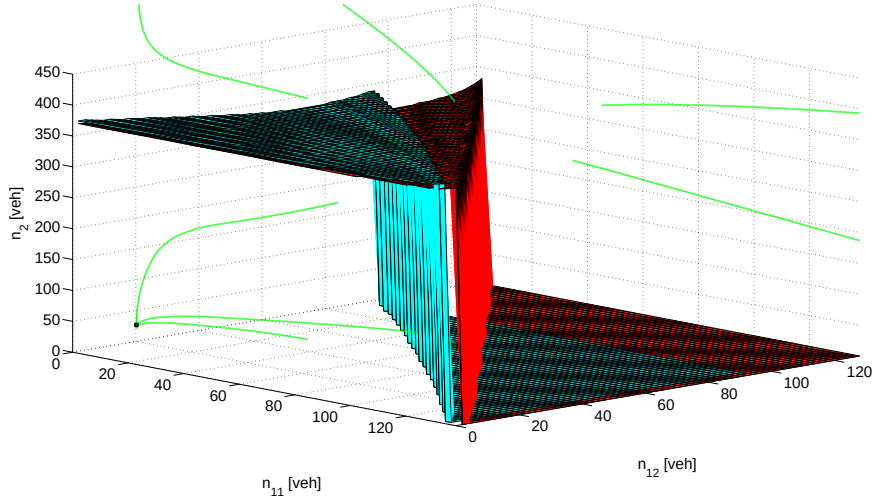

Figure 21: Numerical example 5: RAs boundary surfaces in three states two-region system, $\mathrm{RA}_{u_{\max}}$ surface in red, $\mathrm{RA}_{u_{\min}}$ surface in cyan, and trajectories in green.

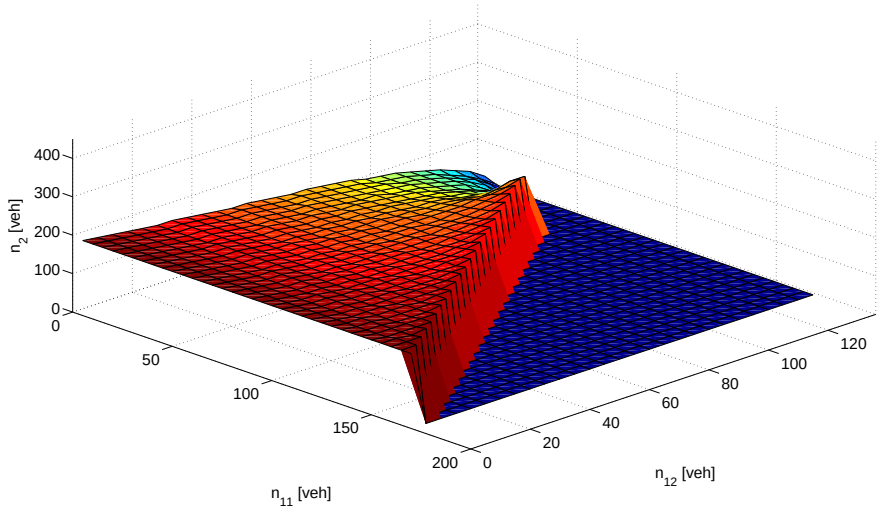

Figure 22: Numerical example 6: $\mathrm{RA}_{u_{\max}}$ surface boundary.

Different shapes of RAs surfaces are expected according to the two states analysis in Section 3.1. For a specific accumulation n_{11} the boundary shape of (n_{12}, n_2)-plane would be one of the three cases a, b, and c shown in Fig. 6, e.g. the $\mathrm{RA}_{u_{\max}}$ and $\mathrm{RA}_{u_{\min}}$ boundary shapes in (n_{12}, n_2)-plane with $n_{11} = 0$ are similar to those in Fig. 10.

Examples 6 and 7 show the effect of different split of demand in region 1 on the $\mathrm{RA}_{u_{\max}}$. In example 6, the demand of region 1 is split $q_{11}(t) = 2/3 \cdot q_1(t)$ and $q_{12}(t) = 1/3 \cdot q_1(t)$, while in example 7 the split is reversed, i.e. $q_{11}(t) = 1/3 \cdot q_1(t)$ and $q_{12}(t) = 2/3 \cdot q_1(t)$. The total demand for region 1 and 2 are $q_1(t) = 0.083[\mathrm{veh/sec}]$ and $q_2(t) = 0.472[\mathrm{veh/sec}]$, while the other input data are similar to those of example 5. Although the total demand q_1 is the same for examples 6 and 7, the $\mathrm{RA}_{u_{\max}}$ shrinks when the exogenous demand $q_{12}(t)$ increases.

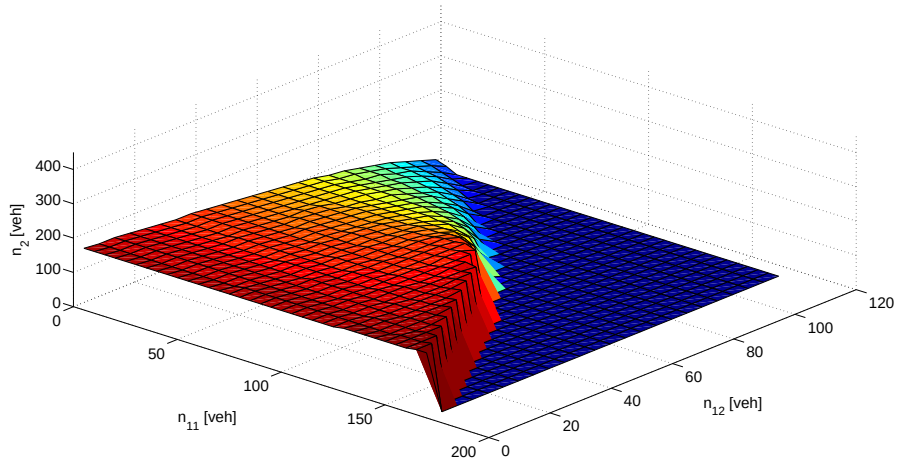

Figure 23: Numerical example 7: $\mathrm{RA}_{u_{\max}}$ surface boundary.

6 Conclusions

In this paper, the optimal control problem for two-region urban cities is formulated where the criterion is to maximize the number of vehicles that complete their trips and reach their destinations by controlling and managing accumulations in the two regions. The macroscopic fundamental diagram for each region is assumed to be known and in triangle shape. One of the two regions has an exogenous demand, i.e. all trips are external, while the second region has an endogenous demand, i.e. all trips are internal.

The dynamic equations of accumulations are analyzed, and equilibrium points of the system are identified. Necessary and sufficient conditions for existence of equilibrium points are derived. Based on the phase portraits of the dynamic equations, a new algorithm is presented to compute numerically and analytically the boundary between stable and unstable regions.

It was proven that the formulated control problem is a feasibility problem, i.e. if an applied control $u(t)$ brings the initial accumulations to a priori optimal stable equilibrium accumulations, then $u(t)$ is an optimal perimeter control. However, if the problem is not feasible for the current accumulations, i.e. the current accumulations belong to unstable region, then the optimal control policy for a relaxed problem should be applied. Hence, based on the stable and unstable regions, a state-feedback strategy is proposed where the optimizing control law of stable region and the optimal control law for unstable region are presented in an analytical feedback form, as a function of current accumulations. In the case when demands are essentially non-constant this solution can be used in the scheme of a predictive control by recalculating control at each new step.

A Trajectory calculation of regions boundaries for cases a, b, and c

A.1 case a

The trajectory from the unstable equilibrium point $(n_{2,\mathrm{eq}}, n_{1,\mathrm{eq}})_{IV}$ to point B is calculated in reverse time (with negative t). Solution in reverse time is equivalent to solution in forward time (with positive t) of the dynamic equation

$$\frac{\mathrm{d}\tilde{n}_1(t)}{\mathrm{d}t} = -\frac{\mathrm{d}n_1(t)}{\mathrm{d}t} \tag{45}$$

$$\frac{\mathrm{d}\tilde{n}_2(t)}{\mathrm{d}t} = -\frac{\mathrm{d}n_2(t)}{\mathrm{d}t} \tag{46}$$

where $\mathrm{d}n_1(t)/\mathrm{d}t$ and $\mathrm{d}n_2(t)/\mathrm{d}t$ are the dynamic equations for state region IV, i.e. substituting (10) into the dynamic equations (5) and (6) with $\mu_1 \leq n_1(t) \leq w_1$ and $\mu_2 \leq n_2(t) \leq w_2$. The direction of ($\tilde{n}_2(t)$, $\tilde{n}_1(t)$) trajectory will be in reverse way, i.e from point B to the unstable equilibrium point $(n_{2,\mathrm{eq}}, n_{1,\mathrm{eq}})_{IV}$.

Given the initial state of the trajectory, i.e. $n_1(0) = \mu_1$ and $n_2(0) = n_{2,B}$, where the starting time is zero, one can integrate (45) and (46), respectively,

$$\tilde{n}_1(t) = w_1 - \frac{q_1 \cdot (w_1 - \mu_1)}{\gamma_1 \cdot u} + (w_1 - \mu_1) \cdot \left(\frac{q_1}{\gamma_1 \cdot u} - 1 \right) \cdot e^{\frac{\gamma_1 \cdot u \cdot t}{\mu_1 - w_1}} \tag{47}$$

$$\begin{aligned} \tilde{n}_2(t) = {} & \frac{e^{\frac{\gamma_1 \cdot u \cdot t}{\mu_1 - w_1}} \cdot (q_1 - \gamma_1 \cdot u) \cdot (\mu_1 - w_1) \cdot (\mu_2 - w_2)}{\gamma_2 \cdot (w_1 - \mu_1) + \gamma_1 \cdot u \cdot (\mu_2 - w_2)} + \\ & + \frac{\mu_2 \cdot (q_1 + q_2) + (\gamma_2 - q_1 - q_2) \cdot w_2}{\gamma_2} + c_2 \cdot e^{\frac{\gamma_2 \cdot t}{\mu_2 - w_2}} \end{aligned} \tag{48}$$

$$c_2 = \frac{\gamma_1 \cdot u \cdot (q_1 - \gamma_1 \cdot u) \cdot w_1 \cdot (\mu_2 - w_2)^2}{(\gamma_2 \cdot \mu_1 + \gamma_1 \cdot u \cdot (w_2 - \mu_2)) \cdot (\gamma_2 \cdot (\mu_1 - w_1) + \gamma_1 \cdot u \cdot (w_2 - \mu_2))} \tag{49}$$

A.2 case b

The trajectory from point C to B is in state region IV, hence the reverse equation system and the trajectory from B to C is the same as in case a, i.e. (47), (48), and (49).

For trajectory CD, the dynamic equations according to (45) and (46) are reversed where $\mathrm{d}n_1(t)/\mathrm{d}t$ and $\mathrm{d}n_2(t)/\mathrm{d}t$ are the dynamic equations for state region III, i.e. substituting (10) into the dynamic equations (5) and (6) with $\mu_1 \leq n_1(t) \leq w_1$ and $0 \leq n_2(t) \leq \mu_2$. The direction of ($\tilde{n}_2(t)$, $\tilde{n}_1(t)$) trajectory will be in reverse way, i.e from C to D.

Given the initial state of the trajectory CD, i.e. $n_1(0) = n_{1,C}$ and $n_2(0) = \mu_2$, where the starting

time is zero, one can integrate (45) and (46), respectively,

$$\tilde{n}_1(t) = \frac{\mu_1 \cdot q_1 - q_1 \cdot w_1 + \gamma_1 \cdot u \cdot w_1}{\gamma_1 \cdot u} + \left(n_{1,C} - w_1 - \frac{q_1 \cdot (\mu_1 - w_1)}{\gamma_1 \cdot u} \right) \cdot e^{\frac{\gamma_1 \cdot u \cdot t}{\mu_1 - w_1}} \tag{50}$$

$$\tilde{n}_2(t) = \mu_2 \cdot \left(\frac{q_1 + q_2}{\gamma_2} + \frac{e^{\frac{\gamma_1 \cdot u \cdot t}{\mu_1 - w_1}} \cdot (\mu_1 \cdot q_1 - q_1 \cdot w_1 + \gamma_1 \cdot u \cdot (w_1 - n_{1,C}))}{\gamma_1 \cdot \mu_2 \cdot u + \gamma_2 \cdot (w_1 - \mu_1)} \right) + c_2 \cdot e^{\frac{\gamma_2 \cdot t}{\mu_2}} \tag{51}$$

$$c_2 = \mu_2 \cdot \left(1 - \frac{q_1 + q_2}{\gamma_2} - \frac{q_1 \cdot (\mu_1 - w_1) + \gamma_1 \cdot u \cdot (w_1 - n_{1,C})}{\gamma_1 \cdot \mu_2 \cdot u + \gamma_2 \cdot (w_1 - \mu_1)} \right) \tag{52}$$

The curves BC and CD for case b are calculated according to the following steps:

1. find T_{BC} [sec] the time instant when trajectory BC enters state region III, i.e. solve numerically $\tilde{n}_2(T_{BC}) = \mu_2$, where $\tilde{n}_2(t)$ is given by (48) and (49),
2. calculate trajectory BC, i.e. calculate $(\tilde{n}_1(t), \tilde{n}_2(t))$ for $t = 0 \rightarrow T_{BC}$ according to (47), (48), and (49).
3. save point $C = (n_{2,C}, n_{1,C}) = (\mu_2, \tilde{n}_1(T_{BC}))$,
4. find T_{CD} [sec] the time instant when trajectory CD intersects $n_2(t) = 0$, i.e. solve numerically $\tilde{n}_2(T_{CD}) = 0$, where $\tilde{n}_2(t)$ is given by (51) and (52),
5. calculate trajectory CD, i.e. calculate $(\tilde{n}_1(t), \tilde{n}_2(t))$ for $t = 0 \rightarrow T_{CD}$ according to (50), (51), and (52).

A.3 case c

In this case, the trajectory BC is in state region I. Hence, given the initial state of the trajectory BC, i.e. $n_1(0) = n_{1,B}$ and $n_2(0) = \mu_2$, where the starting time is zero, one can integrate (45) and (46), respectively, where $\mathrm{d}n_1(t)/\mathrm{d}t$ and $\mathrm{d}n_2(t)/\mathrm{d}t$ are the dynamic equations for state region I, i.e. substituting (10) into the dynamic equations (5) and (6) with $0 \leq n_1(t) \leq \mu_1$ and $0 \leq n_2(t) \leq \mu_2$,

$$\tilde{n}_1(t) = \frac{\mu_1 \cdot q_1}{\gamma_1 \cdot u} + \left(n_{1,B} - \frac{\mu_1 \cdot q_1}{\gamma_1 \cdot u} \right) \cdot e^{\frac{\gamma_1 \cdot u \cdot t}{\mu_1}} \tag{53}$$

$$\tilde{n}_2(t) = \mu_2 \cdot \left(\frac{q_1 + q_2}{\gamma_2} + \frac{e^{\frac{\gamma_1 \cdot t \cdot u}{\mu_1}} \cdot (-\mu_1 \cdot q_1 + \gamma_1 \cdot n_{1,B} \cdot u)}{\gamma_2 \cdot \mu_1 - \gamma_1 \cdot \mu_2 \cdot u} \right) + c_2 \cdot e^{\frac{\gamma_2 \cdot t}{\mu_2}} \tag{54}$$

$$c_2 = \mu_2 \cdot \left(1 - \frac{q_1 + q_2}{\gamma_2} - \frac{\gamma_1 \cdot n_{1,B} \cdot u - \mu_1 \cdot q_1}{\gamma_2 \mu_1 - \gamma_1 \cdot \mu_2 \cdot u} \right) \tag{55}$$

It holds for point C that $\tilde{n}_1(T_{BC}) = \mu_1$, hence, from (53) one can calculate analytically T_{BC}

$$T_{BC} = \ln\left(\frac{\mu_1 \cdot (1 - \frac{q_1}{\gamma_1 \cdot u})}{n_{1,B} - \frac{q_1}{\gamma_1 \cdot u}}\right) \cdot \frac{q_1}{\gamma_1 \cdot u} \tag{56}$$

The trajectory CD is calculated in the same way that was done in case b, however with different initial state. The dynamic equations are reversed according to (45) and (46) where, $\mathrm{d}n_1(t)/\mathrm{d}t$ and $\mathrm{d}n_2(t)/\mathrm{d}t$ are the dynamic equations for state region III, i.e. substituting (10) into the dynamic equations (5) and (6) with $\mu_1 \leq n_1(t) \leq w_1$ and $0 \leq n_2(t) \leq \mu_2$. Given the initial state of the trajectory CD, $n_1(0) = \mu_1$ and $n_2(0) = \tilde{n}_2(T_{BC})$, where the starting time is zero, one can integrate (45) and (46), respectively, and one get same equations as in case b, i.e. (50) and (51), where c_2 is slightly different:

$$c_2 = n_{2,C} - \mu_2 \cdot \left(\frac{q_1 + q_2}{\gamma_2} + \frac{q_1 \cdot (\mu_1 - w_1) + \gamma_1 \cdot u \cdot (w_1 - \mu_1)}{\gamma_1 \cdot \mu_2 \cdot u + \gamma_2 \cdot (w_1 - \mu_1)}\right) \tag{57}$$

The curves BC and CD for case c are calculated according to the following steps:

1. B = $(\mu_2, n_{1,B})$.
2. calculate analytically T_{BC} according to (56).
3. calculate trajectory BC, i.e. calculate $(\tilde{n}_1(t), \tilde{n}_2(t))$ for $t = 0 \rightarrow T_{BC}$ according to (53), (54), and (55).
4. save point $C = (n_{2,C}, n_{1,C}) = (\tilde{n}_1(T_{BC}), \mu_1)$,
5. find T_{CD} [sec] the time instant when trajectory CD intersects $n_2(t) = 0$, i.e. solve numerically $\tilde{n}_2(T_{CD}) = 0$, where $\tilde{n}_2(t)$ is given by (51) and (57),
6. calculate trajectory CD, i.e. calculate $(\tilde{n}_1(t), \tilde{n}_2(t))$ for $t = 0 \rightarrow T_{CD}$ according to (50), (51), and (57).

References

Bemporad, A., G. Ferrari-Trecate and M. Morari (2000) Observability and controllability of piecewise affine and hybrid systems, *IEEE Transactions on Automatic Control*, **45** (10) 1864–1876, OCTOBER 2000.

Boyacı, B. and N. Geroliminis (2011) Exploring the effect of variability of urban systems characteristics in the network capacity, paper presented at *Transportation Research Record 90th Annual Meeting*, Washington, D.C.

Chiang, H.-D. and J. S. Thorp (1989) Stability regions of nonlinear dynamical systems: A constructive methodology, *IEEE Transactions on Automatic Control*, **34** (12) 1229–1241, DEC 1989.

Daganzo, C. F. (2005) A variational formulation of kinematic waves: basic theory and complex boundary conditions, *Transportation Research Part B: Methodological*, **39** (2) 187–196, ISSN 0191-2615.

Daganzo, C. F. (2007) Urban gridlock: Macroscopic modeling and mitigation approaches, *Transportation Research Part B*, **41**, 49–62.

Daganzo, C. F. and N. Geroliminis (2008) An analytical approximation for the macroscopic fundamental diagram of urban traffic, *Transportation Research Part B: Methodological*, **42** (9) 771– 781, ISSN 0191-2615.

Elliott, D. L. (2009) *Bilinear Control Systems*, Springer.

Geroliminis, N. (2007) Increasing mobility in cities by controlling overcrowding, Ph.D. Thesis, University of California, Berkeley.

Geroliminis, N. and C. F. Daganzo (2008) Existence of urban-scale macroscopic fundamental diagrams: some experimental findings, *Transportation Research Part B: Methodological*, **42** (9) 759–770.

Geroliminis, N. and J. Sun (2011) Properties of a well-defined macroscopic fundamental diagram for urban traffic, *Transportation Research Part B*, **45**, 605–617.

Gutman, P.-O. (1981) Stabilizing controllers for bilinear systems, *IEEE Transactions on Automatic Control*, **AC-26** (4) 917–922.

Hassibi, A. and S. Boyd (1998) Quadratic stabilization and control of piecewise-linear systems, paper presented at *the American Control Conference*, 3659–3664.

Helbing, D. (2009) Derivation of a fundamental diagram for urban traffic flow, *The European Physical Journal B*, **70** (2) 229–241.

Izhikevich, E. M. (2007) *Dynamical Systems in Neuroscience: The Geometry of Excitability and Bursting.*, The MIT press.

Ji, Y. and N. Geroliminis (2011) Spatial and temporal analysis of congestion in urban transportation networks, paper presented at *Transportation Research Board 90th Annual Meeting*, Washington, D.C.

Johansson, M. and A. Rantzer (1998) Computation of piecewise quadratic lyapunov functions for hybrid systems, *IEEE Transactions on Automatic Control*, **43**, 555–559.

Khalil, H. K. (2002) *Nonlinear systems*, third edn., Prentice Hall.

Mazloumian, A., N. Geroliminis and D. Helbing (2010) The spatial variability of vehicle densities as determinant of urban network capacity, *Phil. Trans. R. Soc. A*, **368**, 4627–4647.

Mhaskar, P., N. H. El-Farra and P. D. Christofides (2006) Stabilization of nonlinear systems with state and control constraints using Lyapunov-based predictive control, *Systems & Control Letters*, **55**, 650–659.

Pontryagin, L., V. Boltyanskii, R. Gamkrelidze and E. Mishchenko (1962) *The mathematical theory of optimal processes*, Wiley-Interscience, NY.

Tan, W. and A. Packard (2008) Stability region analysis using polynomial and composite polynomial lyapunov functions and sum-of-squares programming, *IEEE Transactions on Automatic Control*, **53** (2) 565–571, MARCH 2008.

Topcu, U. and A. Packard (2009) Local stability analysis for uncertain nonlinear systems, *IEEE Transactions on Automatic Control*, **54** (5) 1042–1047, MAY 2009.